P^{2}C-MUX: Multiplexing with Power and Polarity Coding for Communication Efficiency

Zhao Li, *Senior Member, IEEE,* Lijuan Zhang, Zhangbo Gao, Kang G. Shin, *Life Fellow, IEEE,* Yicheng Liu, *Student Member, IEEE,* Jia Liu, *Senior Member, IEEE,* Hanqing Ding, and Zheng Yan, *Fellow, IEEE*

***Abstract*—As wireless communication systems evolve toward beyond fifth-generation (B5G) and sixth-generation (6G), achieving ultra-high data rates and accommodating massive connectivity present critical challenges for the development of wireless technologies. To meet these challenges, it is important to develop low-cost and high-efficiency multiplexing mechanisms to serve a large number of mobile subscribers with concurrent data streams. We propose a novel scheme, called *Power and Polarity Coding Assisted Multiplexing* (P^{2}C-MUX), to enhance communication efficiency by leveraging existing signals to enable additional data transmissions, *without* increasing power and antenna needs. P^{2}C-MUX first recognizes that the interactions of wireless signals can produce an effective signal for data transmission and then utilizes existing communication signals (ECSs) to achieve additional data transmissions. Specifically, a transmitter (Tx) serves its subscriber (i.e., original receiver (Rx)) with multiple ECSs, while simultaneously transmitting to an additional Rx using P^{2}C-MUX. To achieve this, the Tx adjusts the transmit power and polarity of the ECSs such that these modified/coded ECSs can superimpose to generate desired signals at the additional Rx. In essence, P^{2}C-MUX leverages the interactions among ECSs to enable data transmissions for the additional Rx while maintaining the communication performance of the original Rx, thus enhancing multiplexing efficiency. Furthermore, we extend P^{2}C-MUX to more generalized scenarios involving arbitrary numbers of ECSs, additional users, and additional transmissions per user, as well as various modulation schemes, thus broadening its applicability. We utilize (1) the Universal Software Radio Peripheral (USRP) platform for experimental validation of P^{2}C-MUX's feasibility, and (2) comprehensive MATLAB simulations to demonstrate its effectiveness in improving system spectral efficiency (SE).**

***Index Terms*—Multiplexing, power control, spectral efficiency**

I. Introduction

B5G and 6G wireless communication systems are expected to support data rates of up to 1Tbps, along with user densities reaching as high as 10^7 devices per square kilometer [1]. Multiple-Input Multiple-Output (MIMO) technique, which employs multiple antennas for the transmission and reception of concurrent signals, can enhance the reliability and capacity of wireless data transmissions without requiring additional bandwidth or power consumption. With advancements in MIMO technology, massive MIMO has emerged and used in practical communication systems. This technique leverages hundreds of antenna elements to simultaneously serve dozens of users [2], improving both system capacity and energy efficiency (EE) [3]. However, the numbers of serving users and the concurrent data transmissions supported by a MIMO system are constrained by the numbers of transmitters (Txs) and receivers (Rxs) as well as the number of antennas equipped at both the Txs and Rxs [4], [5]. Additionally, due to limitations in size, power consumption, and hardware costs, mobile terminals are generally unable to accommodate a large number of antennas. Therefore, it is critically important to explore more efficient multiplexing techniques to support a larger number of users while operating within the constraints of a limited number of antennas.

Multiple access (MA) technology is fundamental for enabling the reuse (a.k.a. multiplexing) of communication resources, such as frequency, time, code, and space, among multiple users. Commonly adopted in cellular networks are FDMA, TDMA, CDMA, SDMA, OFDMA, and NOMA. Of these, FDMA, TDMA, CDMA, SDMA, and OFDMA ensure interference-free via exclusive resource allocation, but their ability to accommodate the number of users and concurrent transmissions is limited by the division of communication resources [6]. In contrast, NOMA allows multiple users to simultaneously access the same frequency resource, thus enhancing SE and drawing significant research interests [7]. However, the signal processing techniques employed in NOMA, such as successive interference cancellation (SIC) [8], suffers from error propagation, and the computational complexity of sparse code multiple access (SCMA) increases exponentially with the number of users [9]. These drawbacks highlight the necessity of designing multiplexing schemes with low computational complexity and enhanced user data privacy.

Given the open nature of wireless communication environments, concurrent signal transmissions tend to interact with each other, causing interferences that need to be addressed [10], [11]. On the other hand, some researchers leverage these signal interactions to achieve specific communication objectives, such as enhanced efficiency and secure transmission. For instance, in [12], a recycling signal is intentionally constructed and introduced to the interference environment so that at the

Zhao Li, Lijuan Zhang, Zhangbo Gao, Yicheng Liu, and Zheng Yan are with the School of Cyber Engineering, Xidian University, China. E-mail: zli@xidian.edu.cn; zyan@xidian.edu.cn.

Kang G. Shin is with the Department of Electrical Engineering and Computer Science, The University of Michigan, USA. E-mail: kgshin@umich.edu.

Jia Liu is with the Center for Strategic Cyber Resilience Research and Development, National Institute of Informatics, Japan. E-mail: jliu@nii.ac.jp. *(Corresponding author: Jia Liu)*

Hanqing Ding is with the School of Electronics and Information, Zhengzhou University of Light Industry, China. E-mail: dinghanqing@zzuli.edu.cn.

interfered Rx, the desired signal is formed by superpositioning the recycling signal and interference. This approach effectively utilizes interference to enhance the desired communication. In [13], two coordinated Txs generate separate signals designed to combine at the intended Rx, yielding the desired signal. The intended Rx can recover its desired data from the superimposed signal, while eavesdroppers can only see a scrambled superposition, rendering interception ineffective. This method exploits the randomness of wireless channels and signal interactions to safeguard communication confidentiality. The aforementioned studies demonstrate the potential for intentionally manipulating and utilizing signal interactions to achieve efficient multiplexing.

Based on the above findings, we propose a novel multiplexing scheme called *Power and Polarity Coding assisted Multiplexing* (P^{2}C–MUX). P^{2}C–MUX leverages ECSs intended for data transmission from the original Tx to its Rx to create additional data transmissions by adjusting the transmit power and polarity of the ECSs. Consequently, these coded ECSs are superimposed to produce desired additional communication signals (ACSs) at the additional Rx. This signal-interaction-based approach facilitates flexible capacity enhancement without requiring additional antennas at the Tx/Rx or increased transmit power consumption, thus achieving cost-effective and efficient multiplexing. In the design of P^{2}C–MUX, to prevent polarity coding from misleading the detection of ECSs at the intended Rxs, we embed a 1-bit polarity indicator within each ECS. This polarity bit enables the intended Rxs to correctly decode the data carried in each ECS.

Throughout this paper, we will use the following notations. Vectors and matrices are represented by lower- and upper-case bold letters. $(\cdot)^H$ denotes Hermitian, and $\|\cdot\|$ denotes the Frobenius norm. $(\cdot)^T$ and $(\cdot)^H$ represent the transpose and conjugate transpose, respectively.

II. System Model

We consider a communication system with one original Tx, L original Rxs, and K additional Rxs, each equipped with N_T, N_{RB}, and N_{RC} antennas, respectively, as illustrated in Fig. 1. For simplicity of presentation, our system design begins with $L = K = 1$, where the original Tx, the original Rx, and the additional Rx are designated as Alice, Bob, and Carol, respectively. The extension of this simple system to a more generalized communication system will be elaborated on in Section IV. In this simplified system model, Alice wants to transmit $\mathbf{x}_B = \left[x_{B_1} \cdots x_{B_N}\right]$ and $\mathbf{x}_C = \left[x_{C_1} \cdots x_{C_U}\right]$ to Bob and Carol, respectively, where $N = \min(N_T, N_{RB})$ denotes the number of data streams Alice transmits to Bob, and U ($U \leq N_C$) is the number of additional data streams Alice transmits to Carol. In practice, if $N_T \leq N_{RB}$, all of the spatial degrees of freedom (DoFs) of the channel between Alice and Bob are used for the transmission of $\mathbf{x}_B$. Therefore, it becomes unavailable for Alice to transmit to Carol [14]. In contrast, P^{2}C–MUX allows Alice to transmit N data streams to Bob while simultaneously providing additional data transmissions to Carol. Let P_t denote Alice's transmit power. Alice pre-processes $\mathbf{x}_B$ by jointly applying a precoding matrix $\mathbf{P}_B = \left[\mathbf{p}_{B_1} \cdots \mathbf{p}_{B_N}\right]$, a power coefficient vector $\boldsymbol{\alpha} = \left[\alpha_1 \cdots \alpha_N\right]$, and a polarity coefficient vector $\boldsymbol{\kappa} = \left[\kappa_1 \cdots \kappa_N\right]$, where $0 < \alpha_i < 1$, $\kappa_i \in \{-1, +1\}$, and $\sum_{i=1}^{N} \alpha_i = 1$. The precoded signals are then fed to the transmit antennas for transmission.

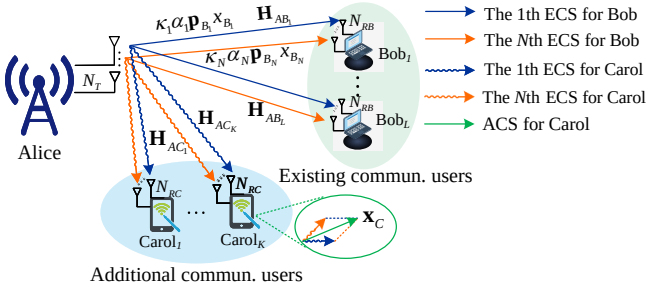

Fig. 1. System model.

$\mathbf{H}_{AB}$ and $\mathbf{H}_{AC}$ denote the channel matrices from Alice to Bob and Carol, respectively. We employ a spatially uncorrelated Rayleigh flat fading channel model to characterize the aforementioned channels, where the elements are independent and identically distributed complex Gaussian random variables with zero mean and unit variance. Channels are mutually independent and exhibit block fading characteristics. Both Bob and Carol are assumed to be able to estimate $\mathbf{H}_{AB}$ and $\mathbf{H}_{AC}$, and then feed this information to Alice. Furthermore, the transmission latency related to channel state information (CSI) feedback and signaling to be negligible compared to the time scale of channel variations [15], [16].

III. Design of P^{2}C–MUX

This section presents the design principle of P^{2}C–MUX under $L = K = 1$. Alice employs M-ary phase shift keying (MPSK) modulation to generate transmitted signals. Without loss of generality, we set $N_T = N_{RB} = 2$ and $N_{RC} \geq 1$. Alice transmits $N = 2$ signals (i.e., ECSs) to Bob and intends to send $U = 1$ additional data stream to Carol. In this case, $\mathbf{x}_C$ simplifies to x_C. Alice performs precoding, which includes spatial precoding using $\mathbf{P}_B$, power and polarity coding (P^{2}C) using $\boldsymbol{\alpha}$ and $\boldsymbol{\kappa}$ on $\mathbf{x}_B$, before transmitting to Bob via multiple antennas. Bob applies a filter matrix $\mathbf{F}_B$ to the observed signal, yielding an estimated signal expressed as:

$$\hat{\mathbf{y}}_B = \mathbf{F}_B^H \begin{bmatrix} \kappa_1\sqrt{\alpha_1 P_t} & 0 \\ 0 & \kappa_2\sqrt{\alpha_2 P_t} \end{bmatrix} \mathbf{H}_{AB}\mathbf{P}_B\mathbf{x}_B + \mathbf{F}_B^H\mathbf{n}_B, \tag{1}$$

where the first term on the right-hand side (RHS) represents the desired signal from Alice after filtering. This desired signal has been pre-processed by $\mathbf{P}_B = [\mathbf{p}_{B_1}\ \mathbf{p}_{B_2}]$, $\boldsymbol{\alpha}$ and $\boldsymbol{\kappa}$, respectively, at Alice. $\mathbf{F}_B = [\mathbf{f}_{B_1}\ \mathbf{f}_{B_2}]$ is used at Bob, and $\mathbf{x}_B = [\mathbf{x}_{B_1}\ \mathbf{x}_{B_2}]^T$ is the desired data for Bob. $\mathbf{n}_B$ denotes the additive white Gaussian noise (AWGN) vector, whose elements have zero mean and variance σ_n^2.

Taking singular value decomposition (SVD)-based precoding and filtering as an example, we apply SVD to $\mathbf{H}_{AB}$ to

obtain $\mathbf{H}_{AB} = \mathbf{U}_{AB}\mathbf{\Sigma}_{AB}\mathbf{V}_{AB}^H$, where $\mathbf{U}_{AB} = [\mathbf{u}_{AB}^{(1)}\ \mathbf{u}_{AB}^{(2)}]$, $\mathbf{\Sigma}_{AB} = \begin{bmatrix} \lambda_{AB}^{(1)} & 0 \\ 0 & \lambda_{AB}^{(2)} \end{bmatrix}$, and $\mathbf{V}_{AB} = [\mathbf{v}_{AB}^{(1)}\ \mathbf{v}_{AB}^{(2)}]$. We then take the two column vectors of $\mathbf{V}_{AB}$ as the precoding vectors for $\mathbf{x}_B$, i.e., letting $\mathbf{p}_{B_1} = \mathbf{v}_{AB}^{(1)}$ and $\mathbf{p}_{B_2} = \mathbf{v}_{AB}^{(2)}$; while the two column vectors of $\mathbf{U}_{AB}$ are used as the filtering vectors $\mathbf{f}_{B_1} = \mathbf{u}_{AB}^{(1)}$ and $\mathbf{f}_{B_2} = \mathbf{u}_{AB}^{(2)}$ for post-processing the signals perceived by Bob.

P^{2}C-MUX manipulates the characteristics of the ECSs sent from Alice and leverages their interactions to produce a desired signal waveform at the additional Rx, Carol. Specifically, Alice adjusts the transmit power and polarity of the two ECSs carrying x_{B_1} and x_{B_2} by applying power coefficients α_1 and α_2, which satisfy $\alpha_1 + \alpha_2 = 1$, along with polarity coefficients κ_1 and κ_2, to them. This adjustment allows the ECSs to superimpose at Carol to form the desired additional signal carrying x_C. Consequently, P^{2}C-MUX increases both the number of users Alice can serve and the number of data transmissions from Alice to the Rxs. Based on the above discussion, we can rewrite Eq. (1) as:

$$\hat{\mathbf{y}}_B = \mathbf{F}_B^H \begin{bmatrix} y_{B_1} \\ y_{B_2} \end{bmatrix} = \begin{bmatrix} \kappa_1\sqrt{\alpha_1 P_t}\lambda_{AB}^{(1)} x_{B_1} \\ \kappa_2\sqrt{\alpha_2 P_t}\lambda_{AB}^{(2)} x_{B_2} \end{bmatrix} + \mathbf{F}_B^H \mathbf{n}_B, \quad (2)$$

where $y_{B_i} = \kappa_i\sqrt{\alpha_i P_t}\mathbf{H}_{AB}\mathbf{p}_{B_i}x_{B_i}$ $(i \in \{1,2\})$. According to Eq. (2), power coding with $\boldsymbol{\alpha}$ does not affect the spatial features of the signals intended for Bob. Therefore, when $\kappa_i = +1$, Bob can correctly recover x_{B_i}. However, in the case of $\kappa_i = -1$, decoding errors will occur at Bob. To address this issue, we will propose an in-band 1-bit polarity coding/decoding method later in this section to avoid decoding errors incurred by the phase inversion.

In what follows, we will present the generation of additional communication signal (ACS) using the ECSs. The signal perceived by Carol can be expressed as:

$$\mathbf{y}_C = \kappa_1\sqrt{\alpha_1 P_t}\mathbf{H}_{AC}\mathbf{p}_{B_1}x_{B_1} + \kappa_2\sqrt{\alpha_2 P_t}\mathbf{H}_{AC}\mathbf{p}_{B_2}x_{B_2} + \mathbf{n}_C, \quad (3)$$

where $\mathbf{n}_C$ denotes the AWGN vector at Carol.

Carol utilizes a filtering vector $\mathbf{f}_C^H$ to post-process $\mathbf{y}_C$. This filtering vector can be obtained by applying SVD to $\mathbf{H}_{AC}$ and selecting the first column of its right singular matrix. Consequently, to recover x_C at Carol, the first two terms on the RHS of Eq. (3) must satisfy:

$$\mathbf{f}_C^H(\kappa_1\sqrt{\alpha_1 P_t}\mathbf{H}_{AC}\mathbf{p}_{B_1}x_{B_1} + \kappa_2\sqrt{\alpha_2 P_t}\mathbf{H}_{AC}\mathbf{p}_{B_2}x_{B_2}) = \gamma x_C, \quad (4)$$

where γ is a positive real coefficient indicating that the data recovered by Carol is the desired data x_C scaled by γ. It is important to note that although Carol is equipped with multiple antennas, she does not process the individual ECS components separately. Instead, she treats the superimposed ECSs as a whole for processing. Since either a data symbol or a complex signal can be represented by its amplitude and phase [17], we can define $x_C = \rho_C e^{j\theta_C}$; while the ECS without P^{2}C, after filtering at Carol, can be expressed as $\sqrt{P_t}\mathbf{f}_C^H\mathbf{H}_{AC}\mathbf{p}_{B_i}x_{B_i} = s_i = \rho_{B_i}e^{j\theta_{B_i}}$, where ρ_i and θ_i $(i \in \{1,2,C\})$ represent the amplitude and phase of the data and ECS, respectively. Therefore, We can simplify Eq. (4) to:

$$\kappa_1\sqrt{\alpha}_1\rho_{B_1}e^{j\theta_{B_1}} + \kappa_2\sqrt{\alpha}_2\rho_{B_2}e^{j\theta_{B_2}} = \gamma\rho_C e^{j\theta_C}. \quad (5)$$

Fig. 2 illustrates the principle of power coding (PowC) in P^{2}C-MUX. For simplicity of presentation, we set $\kappa_i = +1$ in the following discussion, and will address the polarity coding (PolC) later in this section. Without loss of generality, we assume Alice employs QPSK modulation to transmit to both Bob and Carol. In the figure, the two ECSs, denoted as s_1 (i.e., vector $\overrightarrow{OA}$) and s_2 (i.e., vector $\overrightarrow{OB}$), combine at Carol to form her desired signal carrying x_C. For the purpose of illustration, we consider x_C corresponding to a constellation point in the first quadrant. In the absence of PowC, the superposition of s_1 and s_2 results in vector $\overrightarrow{OC}$, whose phase deviates from the desired phase θ_C. By introducing power coefficients α_1 and α_2 to adjust the amplitudes of s_1 and s_2, the ECSs become vectors $\overrightarrow{OA'}$ and $\overrightarrow{OB'}$. As the figure shows, these adjusted ECSs can produce vector $\overrightarrow{OC'}$, which aligns in phase with x_C. Thus, without increasing the number of transmit antennas at Alice, she can serve Bob with N data streams while simultaneously providing an additional data transmission to Carol, thereby enhancing her capability to serve multiple subscribers and improving the system's SE.

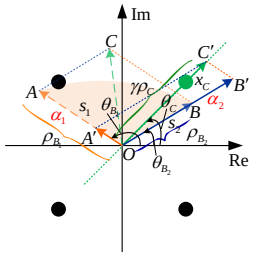

Fig. 2. Illustration of the power coding (PowC) in P^{2}C-MUX.

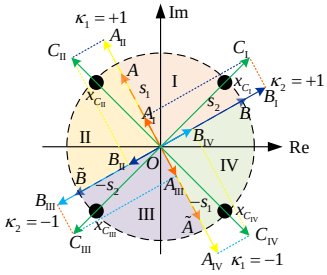

Fig. 3. Illustration of the P^{2}C in P^{2}C-MUX.

Next, we present how to determine α_i under the condition $\kappa_i = +1$. According to Euler's formula, we rewrite Eq. (5) as:

$$\sum_{i=1}^{2}\sqrt{\alpha_i}\rho_{B_i}(\cos\theta_{B_i} + j\sin\theta_{B_i}) = \gamma\rho_C(\cos\theta_C + j\sin\theta_C). \quad (6)$$

From Eq. (6), and using $\alpha_2 = 1 - \alpha_1$, we can obtain:

$$\begin{cases} \sqrt{\alpha_1}\rho_{B_1}\cos\theta_{B_1} + \sqrt{1-\alpha_1}\rho_{B_2}\cos\theta_{B_2} = \gamma\rho_C\cos\theta_C \\ \sqrt{\alpha_1}\rho_{B_1}\sin\theta_{B_1} + \sqrt{1-\alpha_1}\rho_{B_2}\sin\theta_{B_2} = \gamma\rho_C\sin\theta_C \end{cases}. \quad (7)$$

Then, we can derive $\gamma = \frac{\sqrt{\alpha_1}\rho_{B_1}\sin\theta_{B_1} + \sqrt{1-\alpha_1}\rho_{B_2}\sin\theta_{B_2}}{\rho_C\sin\theta_C}$ from the second equation in Eq. (7). Substituting this expression into the first equation of (7) yields:

$$\begin{aligned} &\sqrt{\alpha_1}(\rho_{B_1}\cos\theta_{B_1}\sin\theta_C - \rho_{B_1}\sin\theta_{B_1}\cos\theta_C) \\ &= \sqrt{1-\alpha_1}(\rho_{B_2}\sin\theta_{B_2}\cos\theta_C - \rho_{B_2}\cos\theta_{B_2}\sin\theta_C). \end{aligned} \quad (8)$$

By squaring both sides of Eq. (8), we can solve for α_1:

$$\alpha_1 = B^2/(A^2 + B^2), \quad (9)$$

where $A = \rho_{B_1}\cos\theta_{B_1}\sin\theta_C - \rho_{B_1}\sin\theta_{B_1}\cos\theta_C$ and $B = \rho_{B_2}\sin\theta_{B_2}\cos\theta_C - \rho_{B_2}\cos\theta_{B_2}\sin\theta_C$. Upon determining α_1, we can further calculate α_2 as:

$$\alpha_2 = 1 - \alpha_1 = A^2/(A^2 + B^2). \tag{10}$$

The above discussion demonstrates how Carol's desired signal can be constructed by combining s_1 and s_2 using the PowC method. However, in practice, due to the randomness of $\mathbf{x}_B$ and x_C, relying solely on PowC may not suffice to achieve the desired signal at Carol. For instance, as shown in Fig. 2, PowC is applicable only when x_C falls within the sector defined by the vectors $\overrightarrow{OA}$ and $\overrightarrow{OB}$. In other cases, we must introduce an additional DoF to adjust the ECSs so as to ensure the production of x_C. In the design of P^{2}C–MUX, we utilize signal polarity as the adjustable parameter, referred to as polarity coding (PolC). Clearly, when the polarity of ECSs can be adjusted, we can ensure that regardless of x_C's location in the complex plane, the sector defined by the adjusted ECSs using P^{2}C will encompass x_C, making the P^{2}C–MUX effective.

Fig. 3 illustrates the principle of generating Carol's desired signal through P^{2}C. Without loss of generality, we consider the scenario where s_1 and s_2 are positioned in the second and first quadrants, respectively, while x_C can be located in any of the four quadrants. Without employing P^{2}C, the ECGs (i.e., s_1 and s_2) are represented by the vectors $\overrightarrow{OA}$ and $\overrightarrow{OB}$, respectively. In case I, x_C lies in the first quadrant, and its phase falls within sector I which is defined by $\overrightarrow{OA}$ and $\overrightarrow{OB}$. By setting the polarity coefficients to $+1$, PowC ensures that the modified ECSs $\overrightarrow{OA_{\rm I}}$ and $\overrightarrow{OB_{\rm I}}$ combine to produce the vector $\overrightarrow{OC_{\rm I}}$ aligning with x_C, satisfying $+\sqrt{\alpha_1}s_1 + \sqrt{\alpha_2}s_2 = \gamma x_C$. In case II, where x_C lies in the second quadrant, merely adjusting the strengths of s_1 and s_2 is insufficient to obtain x_C. In this case, we can reverse the polarity of s_2 by setting $\kappa_2 = -1$ to obtain vector $\overrightarrow{OB}$. This allows $+s_1$ and $-s_2$ to define region II, which encompasses x_C. Consequently, desired ACS can be generated. Cases III and IV are analogous to Case II. Specifically, in Case III, both κ_1 and κ_2 are set to -1, while in case IV, we set $\kappa_1 = -1$ and $\kappa_2 = +1$. Based on the above analysis, it is evident that by applying P^{2}C we can produce an ACS that carries x_C via the combination of ECSs.

When applying P^{2}C–MUX, we should first determine $\boldsymbol{\kappa}$, followed by $\boldsymbol{\alpha}$. As mentioned above, $\boldsymbol{\kappa}$ depend on the phase relationships of x_C, s_1 and s_2, i.e., θ_C, θ_{B_1} and θ_{B_2}. Note that all of these phases are in the range of $[0, 2\pi)$. Without loss of generality, we assume $\theta_{B_2} > \theta_{B_1}$. We can then determine $\boldsymbol{\kappa}$ according to Table I. After obtaining $\boldsymbol{\kappa}$, we can further employ the method presented in Eqs. (9) and (10) to calculate $\boldsymbol{\alpha}$. Now both $\boldsymbol{\kappa}$ and $\boldsymbol{\alpha}$ are ready for the application of P^{2}C–MUX.

The use of PolC ensures the feasibility of P^{2}C–MUX, but alterations of the polarity of the ECSs may lead to decoding errors for Bob. So, it is critical to use a cost-effective way of delivering polarity information to Bob to help him accurately decode the polarity-modified ECSs. Thus, besides determining $\boldsymbol{\kappa}$, PolC should also involve the joint encoding/decoding of the polarity coefficient and the desired information at Alice/Bob.

TABLE I
THE CALCULATION OF POLARITY COEFFICIENTS.

Relationships of θ_C, θ_{B_1} and θ_{B_2}		κ_1	κ_2
$\theta_{B_2} - \theta_{B_1} < \pi$	$0 \le \theta_C - \theta_{B_1} < \theta_{B_2} - \theta_{B_1}$	$+1$	$+1$
	$\theta_{B_2} - \theta_{B_1} \le \theta_C - \theta_{B_1} < \pi$	-1	$+1$
	$\pi \le \theta_C - \theta_{B_1} < \theta_{B_2} - \theta_{B_1} + \pi$	-1	-1
	$\theta_{B_2} - \theta_{B_1} + \pi \le \theta_C - \theta_{B_1} < 2\pi$	$+1$	-1
$\theta_{B_2} - \theta_{B_1} > \pi$	$0 \le \theta_C - \theta_{B_1} < \theta_{B_2} + \pi - \theta_{B_1}$	$+1$	-1
	$\theta_{B_2} + \pi - \theta_{B_1} \le \theta_C - \theta_{B_1} < \pi$	-1	-1
	$\pi \le \theta_C - \theta_{B_1} < \theta_{B_2} - \theta_{B_1}$	-1	$+1$
	$\theta_{B_2} - \theta_{B_1} \le \theta_C - \theta_{B_1} < 2\pi$	$+1$	$+1$

In what follows, we will propose 1-bit in-band signaling to address this issue, where Alice encodes the polarity information into the data symbols transmitted to Bob. Bob can then retrieve this information and use it to recover his desired data. Taking the case where both s_1 and s_2 employ QPSK modulation as an example, Alice allocates 1 bit in each QPSK symbol to indicate the polarity of that symbol (a.k.a. waveform). Without loss of generality, we define the least significant bit (LSB) of the 2-bit QPSK symbol as the polarity bit. (Polarity bits "0" and "1" represent positive and negative polarity, respectively.) When the polarity of a symbol carried in an ECS is inverted (i.e. $\kappa_i = -1$), its polarity bit is set to "1". Upon detection, Bob must invert the remaining data bits of this symbol to retrieve the correct information. Conversely, if the polarity remains unchanged (i.e., $\kappa_i = +1$), the polarity bit is set to "0", allowing Bob to directly extract the decoded data bits as his desired information. The encoding and decoding rules for the polarity bit and desired data under QPSK are summarized in Table II.

TABLE II
ENCODING/DECODING RULES FOR POLARITY BIT AND DESIRED DATA.

Desired data for transmission	0	0	1	1
Polarity of ECS	$+1$	-1	$+1$	-1
Polarity bit	0	1	0	1
Encoded QPSK data with polarity bit	00	11	10	01
Decoded data for reception	0	0	1	1

As observed from Table II, the relationship among the desired data, the polarity bit, and the polarity-encoded data can be expressed as:

$$x_{B_i}^{(l)} \leftarrow x_{B_i}^{(l)} \oplus x_{B_i}^{\log_2 M_{B_i}},\ l \in \{1, \cdots, \log_2 M_{B_i} - 1\}, \tag{11}$$

where $\oplus$ denotes logic exclusive-OR (XOR) operation. $x_{B_i}^{(l)}$ on the RHS of Eq. (11) represents the l-th bit of a desired data symbol on the i-th ECS before polarity encoding[1]. M_{B_i} represents the modulation order of the i-th ECS. The term $x_{B_i}^{\log_2 M_{B_i}}$ refers to the LSB of a data symbol, which is utilized as the polarity bit. Conversely, $x_{B_i}^{(l)}$ on the left-hand side (LHS) of Eq. (11) represents the l-th bit of a data symbol on the i-th ECS after polarity encoding. The symbol $\leftarrow$ indicates that $x_{B_i}^{(l)}$ is substituted with the encoded result $x_{B_i}^{(l)} \oplus x_{B_i}^{\log_2 M_{B_i}}$. In practice, multiple ECSs may employ various modulation

[1]Here we use the term "polarity encoding" to refer to the process of encoding the polarity coefficient into the transmitted data symbol, as well as the joint encoding of the polarity coefficient and the desired data information at Alice.

schemes, and hence the above polarity encoding can be directly applied.

Bob's decoding process can be implemented by performing a bit-wise XOR operation between the received data bits and the associated polarity bit:

$$\hat{x}_{B_i}^{(l)} \leftarrow \hat{x}_{B_i}^{(l)} \oplus \hat{x}_{B_i}^{\log_2 M_{B_i}},\ l \in \{1, \cdots, \log_2 M_{B_i} - 1\}, \quad (12)$$

where $\hat{x}_{B_i}^{(l)}$ on the RHS of Eq. (12) denotes the l-th data bit of the polarity-encoded symbol recovered by Bob from the i-th ECS, and $\hat{x}_{B_i}^{\log_2 M_{B_i}}$ represents the decoded polarity bit. Eq. (12) indicates that the l-th data bit of the desired symbol (i.e., $\hat{x}_{B_i}^{(l)}$ on the LHS of Eq. (12)) is obtained by calculating $\hat{x}_{B_i}^{(l)} \oplus \hat{x}_{B_i}^{\log_2 M_{B_i}}$. For various modulation schemes across different ECSs, the above polarity decoding methods can be applied directly.

To this end, with P^{2}C–MUX, Alice can simultaneously transmit $N = 2$ parallel data streams to Bob while providing $U = 1$ additional data transmission to Carol.

IV. Generalization of P^{2}C–MUX

We first present the design of P^{2}C–MUX under more general modulation schemes and then discuss the implementation of P^{2}C–MUX with arbitrary numbers of ECSs, ACSs, and additional Rxs.

A. Extended Design of P^{2}C–MUX for General Modulation Schemes

In the design discussed thus far, both the ECS and ACS are assumed to employ the same-order MPSK modulation. However, in practice, multiple ECSs may use MPSK with different orders, and the modulation order of the ACS may also differ from that of the ECS. Under such conditions, the P^{2}C–MUX proposed in Section III can be directly applied. Moreover, when the ECS employs MPSK, the P^{2}C–MUX can accommodate ACS using multiple quadrature amplitude modulation (MQAM). This is because the P^{2}C does not modify the phase of ECS intended for Bob, ensuring the correct decoding of ECS at Bob. On the other hand, P^{2}C enables the combination of multiple ECSs to yield the desired MQAM-modulated signal. In what follows, we will present the extended design of P^{2}C–MUX when the ECS utilizes MPSK and the ACS adopts MQAM. Unlike MPSK, where only the signal phase carries information, in MQAM, both the phase and amplitude of the signal convey information. Therefore, when generating the desired signal for Carol, it is crucial to align the constellation point associated with the combined signal as closely as possible to the standard constellation point corresponding to the desired data. Then, to achieve x_C, we must satisfy $\kappa_1\sqrt{\alpha_1}s_1 + \kappa_2\sqrt{\alpha_2}s_2 = x_C$, which is directly derived from Eq. (4).

It should be noted that when all of the ECSs employ MQAM, Alice will be unable to leverage P^{2}C–MUX to provide additional data transmission services. This limitation arises because PowC alters the amplitude of the ECS, and in MQAM, the amplitude carries information. So, PowC will cause errors in Bob's decoding of the ECS. Consequently, to avoid disrupting the communication from Alice to Bob, when all of the ECSs use signal amplitude to convey information, P^{2}C–MUX should not be used. However, whenever there exists at least one ECS using MPSK, P^{2}C–MUX is applicable.

B. Extended Design of P^{2}C–MUX under Arbitrary Numbers of ECSs, ACSs, and Additional Rxs

In Section III, we have demonstrated that an ACS for an additional Rx can be generated from two ECSs. In practice, there may be a larger number of ECSs, and both the number of additional Rxs and the number of ACSs per additional Rx may exceed one. Here we will discuss the design of P^{2}C–MUX in more generalized cases where the numbers of ECSs N, additional Rxs K, and ACSs for each additional Rx U can take arbitrary values. For simplicity, we will consider the case where Alice, Bob and Carol adopt MPSK.

1) Design of P^{2}C–MUX under $N > 2$, $K = 1$ and $U = 1$: In practice, Alice may serve a single or multiple original Rxs with $N > 2$ ECSs. In such cases, P^{2}C–MUX can be directly utilized by employing all of the ECSs to generate the ACS. Note that if the ECSs are from various original Txs, they must cooperate with each other to produce the ACS at the additional Rx. This requirement imposes some cooperation costs among multiple original Txs. The implementation of P^{2}C–MUX under $N > 2$, $K = 1$ and $U = 1$ is detailed as follows.

According to Section III, the estimated signal after receiving filtering at Carol should satisfy:

$$\sum\nolimits_{i=1}^{N} \kappa_i \sqrt{\alpha_i P_t} \mathbf{f}_C^H \mathbf{H}_{AC} \mathbf{p}_{B_i} x_{B_i} = \gamma x_C. \quad (13)$$

When applying P^{2}C–MUX, we can partition the N ECSs into two groups. The ECSs in each group can then be equivalent to an effective ECS [18], denoted as s_{eq1} and s_{eq2}, respectively. The P^{2}C–MUX presented in Section III can then be applied directly to determine the power and polarity coefficients. As a result, by applying the above coefficients to the ECSs forming s_{eq1} and s_{eq2}, Eq. (13) can be satisfied.

2) Design of P^{2}C–MUX under $N > 2$, $K > 1$ and $U = 1$: When multiple ECSs are available, Alice can employ P^{2}C–MUX to provide data services to multiple additional Rxs. Here we assume that Alice uses N ECSs to serve $K > 1$ additional Rxs, each with a single additional data stream. Both the ECS and ACS adopt MPSK modulation. Similar to Eq. (13), the estimated signal at the additional Rx indexed by j ($j \in \{1, \cdots, K\}$) (i.e., Carol$_j$) should satisfy:

$$\sum\nolimits_{i=1}^{N} \kappa_i \sqrt{\alpha_i P_t} \mathbf{f}_{C,j}^H \mathbf{H}_{AK,j} \mathbf{p}_{B_i} x_{B_i} = \gamma_j x_{C_j}, \quad (14)$$

where $\mathbf{f}_{C,j}^H$ denotes the receive filter vector of Carol$_j$. $\mathbf{H}_{AK,j}$ represents the channel between Alice and the Carol$_j$, and x_{C_j} is the data that Alice intends to transmit to Carol$_j$. Since all of the estimated ACSs at the K additional Rxs must satisfy Eq. (14), these K equations must be considered jointly, along with the constraints $\sum_{i=1}^{N} \alpha_i = 1$ and $\alpha_i > 0$. By using the method presented in Section III, $\boldsymbol{\alpha}$ and $\boldsymbol{\kappa}$ can be solved.

TABLE III
PARAMETER SETTINGS OF P^{2}C−MUX.

Carrier freq.	Symbol rate	Interpolation factor	Sampling rate (base-band)	Roll-off factor of raised cosine filter	Transmit gain of each Tx
915MHz	0.2MBaud	8	0.4MBaud	0.5	{10dB,13dB,16dB}

It is important to note that under $N > 2$, $K > 1$ and $U = 1$, each additional Rx receives the superposition of all N ECSs. Carol$_j$ applies a receive filter to process the combination of the N ECSs, thereby recovering $\gamma_j x_{C_j}$. Moreover, as indicated by Eq. (14), each additional Rx can recover its desired data without experiencing interference, due to the randomness and independence of the channel conditions associated with the Rxs. When $N > 1$, $K = 1$, and $U > 1$, this scenario is similar to that in subsection 2). Given the consistency in implementation principles with subsection 2), we omit further elaboration.

3) Feasibility Analysis of P^{2}C−MUX*:* In practice, different ACSs may impose various and even conflicting power and polarity requirements on the same ECS. In such cases, $\boldsymbol{\alpha}$ and $\boldsymbol{\kappa}$ become unsolvable, rendering P^{2}C−MUX infeasible. A qualitative analysis of the impact of these parameters on the feasibility of P^{2}C−MUX (i.e. p_{P^2C-MUX}) is presented below.

First, we consider the impact of N on p_{P^2C-MUX}. Given fixed values of K, U, M_B, and M_C, a small N limits the number of adjustable $\boldsymbol{\alpha}$ and $\boldsymbol{\kappa}$. As a result, the diversity of the combination of ECSs is reduced, leading to a decrease in p_{P^2C-MUX}. To facilitate the application of P^{2}C−MUX, we should, therefore, use as many ECSs as possible.

Second, we discuss the impact of K and U on p_{P^2C-MUX}. As mentioned earlier, various and conflicting power and polarity requirements on the same ECS can hinder the applicability of P^{2}C−MUX. Consequently, when K and/or U are small, the likelihood of such conflicts is low, which leads to a higher p_{P^2C-MUX}. Conversely, as K and/or U increases, conflicts become more likely, thus reducing the feasibility of P^{2}C−MUX. An extreme case arises when $K = U = 1$; in such a case, no power and polarity conflict occurs, resulting in $p_{P^2C-MUX} = 1$.

Third, we examine the influence of M_B and M_C on p_{P^2C-MUX}. Note that M_B has no impact on p_{P^2C-MUX}, because, regardless of the value of M_B, the statistical characteristics of the ECSs observed by the additional Rx remain unchanged due to the statistical independence between $\mathbf{H}_{AB}$ and $\mathbf{H}_{AC}$. Therefore, p_{P^2C-MUX} is independent of M_B. In contrast, under $K > 1$ and $U > 1$, a greater M_C tends to reduce p_{P^2C-MUX}. This is because, as M_C increases, the constellation of ACS becomes more diverse. This increased diversity raises the difficulty of designing a single set of $\boldsymbol{\alpha}$ and $\boldsymbol{\kappa}$ that can simultaneously satisfy the requirements of multiple ACSs. So, p_{P^2C-MUX} decreases as M_C increases.

In summary, p_{P^2C-MUX} grows with the increase of N, and reduces with the increase of K, U and M_C, while remaining unaffected by M_B.

V. EVALUATION

We first validate the feasibility of P^{2}C−MUX by implementing it on the Universal Software Radio Peripheral (USRP) platform.Then, we evaluate the performance of P^{2}C−MUX through MATLAB simulations.

A. Hardware Experimentation

We employ a USRP X310 device to serve as the original Tx (Alice) and a USRP B210 device to act as the additional Rx (Carol), to verify that by using P^{2}C−MUX, Alice can generate an ACS at Carol from the two ECSs sent from her.[2] In the experiment, we have Alice employ QPSK to generate the ECSs, while the additional data transmission from Alice to Carol uses 16QAM. The experimental setup is illustrated in Fig. 4, where the USRP X310 device is connected to a terminal (PC1), which controls the USRP X310 to send two QPSK signals. The USRP B210 device is connected to another terminal (PC2), and under its control, the B210 performs signal reception and data demodulation in 16QAM mode. It should be noted that this experimental setup is fundamentally different from a conventional 2×1 MISO system, where all transmit antennas jointly process and send the data symbols. In contrast, in the experiment, each of the two transmit antennas in the X310 independently transmits a distinct data stream to Carol. For simplicity, we deploy the additional Rx (Carol) on the mid-perpendicular line between the two Tx antennas. Consequently, the two signals sent simultaneously from Alice can reach Carol synchronously. This symmetric deployment also helps mitigate the impact of fading differences between the two transmission links on the reception at Carol, ensuring that both ECSs experience approximately identical fading. The main parameters used in the experiment are summarized in Table III.

In the experiment, PC1 controls the USRP X310 to serve as Alice, generating two QPSK-modulated ECSs, s_{B_1} and s_{B_2}, carrying data x_{B_1} and x_{B_2}, respectively. These two ECSs share the same phase set $\{\frac{\pi}{4}, \frac{3\pi}{4}, \frac{5\pi}{4}, \frac{7\pi}{4}\}$. At Carol, the two ECSs are superimposed to form an ACS exhibiting a 16QAM constellation. To recover the additional data x_C from the received combination of ECSs, Carol first estimates the equivalent CSI between herself and Alice using a known pilot sequence[3] prior to the data transmission. Based on the estimated CSI, Carol applies appropriate channel compensation, which includes frequency and phase offsets correction as well as automatic gain control (AGC), and employs a 16QAM demodulator to decode the superimposed ECSs.

In our experiment design, since signal polarity is not intuitively observable in the constellation map, we primarily focus on verifying the feasibility of generating the desired

[2]Since the P^{2}C−MUX primarily focuses on utilizing the ECSs to produce additional data transmission, the transmission between Alice and Bob is not the key aspect of the proposed method. Therefore, in the experimental setup, we do not take the original Rx (Bob) into account.

[3]In the experiment, a Barker code is employed as the pilot sequence for synchronization and channel estimation.

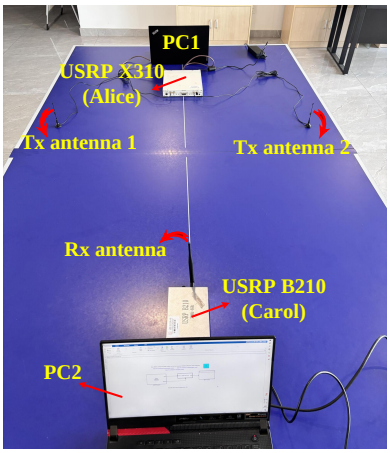

Fig. 4. Hardware implementation of P^{2}C-MUX.

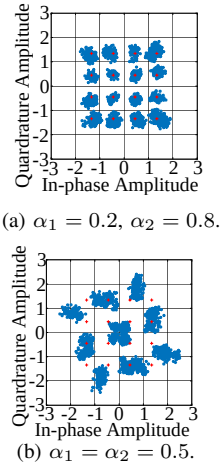

(a) $\alpha_1 = 0.2$, $\alpha_2 = 0.8$.

(b) $\alpha_1 = \alpha_2 = 0.5$.

Fig. 5. Carol's constellations under various power coefficients.

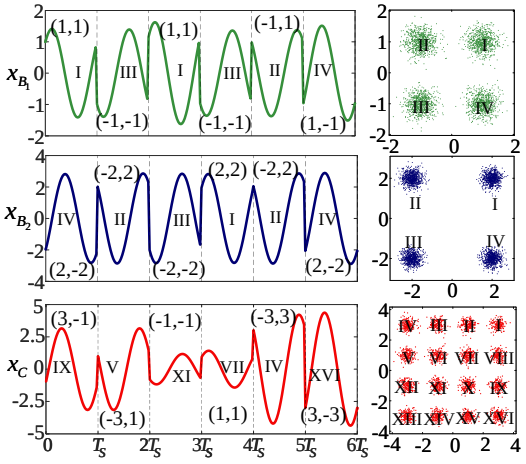

Fig. 6. Waveforms and constellations of 6 QPSK symbols carried in ECSs and decoded 16QAM symbols carried in ACS.

ACS through PowC. We examine the superposition behavior of the two ECSs (denoted as s_1 and s_2) at Carol by setting their transmit gains to $(10\text{dB}, 16\text{dB})$ and $(13\text{dB}, 13\text{dB})$, respectively. Under these conditions, the corresponding power coefficients (α_1, α_2) of the ECSs are equivalent to (0.2, 0.8) and $(0.5, 0.5)$, respectively.

Fig. 5 illustrates the constellation map of the combined ECSs at Carol under various power coefficients. As Fig. 5(a) shows, by setting the amplitude of s_2 to be twice that of s_1, the two QPSK-modulated ECSs can produce a standard 16QAM constellation, which is consistent with the implementation of 16QAM [13]. When the transmit gains of the two ECSs are set to be the same, the distances between the two transmit antennas and Carol are also identical, resulting in the power coefficients (α_1, α_2) being equivalent to $(0.5, 0.5)$. In this case, the superposition of the two ECSs at Carol yields an attenuated constellation.[4] From this constellation, Carol cannot recover x_C intended for her.

Fig. 5 confirms that with appropriate PowC, using ECSs can generate the desired ACS. To further validate that Carol can decode her desired data x_C from the combined ECSs, we plot in Fig. 6 the waveforms of some data symbols carried in the ECSs, denoted as x_{B_1} and x_{B_2}, along with the waveforms of corresponding data symbols decoded from the combined ECSs, denoted as x_C. For clarity, we also plot the constellations corresponding to the QPSK-modulated symbols and demodulated 16QAM symbols in the figure. In the experiment, we set the transmit gains of the two ECSs to 10 dB and 16 dB, respectively, to ensure that the amplitude of s_2 is twice that of s_1. Without loss of generality, Fig. 6 displays six symbol periods, where T_S denotes the length of a data symbol, with each symbol waveform annotated with its corresponding I/Q coordinates in the complex plane. Taking the first symbol period as an example, we can see in the upper subplot that x_{B_1} exhibits I/Q coordinates of $(1, 1)$, while in the middle subplot, x_{B_2} has coordinates of $(2, -2)$. From this, we can derive that the combination of the two ECSs yields I/Q coordinates of $(3, -1)$, which is consistent with the coordinates of the first symbol shown in the lower subplot. This relationship is also reflected in the constellation maps on the right side of Fig. 6. Specifically, x_{B_1} with coordinates $(1, 1)$ corresponds to the point located at "I" in the upper constellation, while x_{B_2} with coordinates $(2, -2)$ corresponds to the point located at "IV" in the middle constellation. Their combination yields x_C with coordinates $(3, -1)$ at the "IX" point in the lower constellation. In summary, these experiments corroborate the effectiveness of P^{2}C-MUX.

[4]Due to the inappropriate settings of (α_1, α_2), the combined pilot at Carol becomes scrambled, preventing her from accurately estimating the equivalent channel between herself and Alice, and from compensating for the phase offset. Consequently, the constellation appears rotated.

B. MATLAB Simulation

We also evaluate the performance of P^{2}C-MUX through MATLAB simulations. In the simulation setup, both Alice and Bob are equipped with $N_A = N_B \in \{2, 3, 4, 5, 6\}$ antennas, while Carol is equipped with $N_C \in \{1, 2, 3\}$ antennas. We define the transmit power of Alice, denoted as P_t, normalized by the noise power σ_n^2, as $\epsilon = 10\lg(P_t/\sigma_n^2)$dB, and set $\epsilon \in [5, 25]$dB in the simulation. We employ Monte Carlo simulation with 10^4 trials. In each trial, the channel matrices $\mathbf{H}_{AB}$ and $\mathbf{H}_{AC}$ are generated following the channel model presented in Section II.

First, we compare the SE of P^{2}C-MUX with that of zero-forcing beamforming (ZFBF) [18] and non-P^{2}C scheme. In this simulation, we set $N_A = N_B = 2$ and $N_C = 1$. Both the ECSs and ACS employ QPSK for data transmission. In the simulation of P^{2}C-MUX, we only need to ensure that the superposition of ECSs is in phase with that of the desired ACS. In contrast, for ZFBF, Alice transmits a single precoded data stream to Bob and Carol separately, allowing each Rx to receive its desired signal without interference. In the simulation of non-P^{2}C, Alice employs spatial multiplexing (SM) to transmit two data streams to Bob. Since there is no extra DoF available, Alice cannot provide additional data transmission services to Carol. Consequently, the system SE

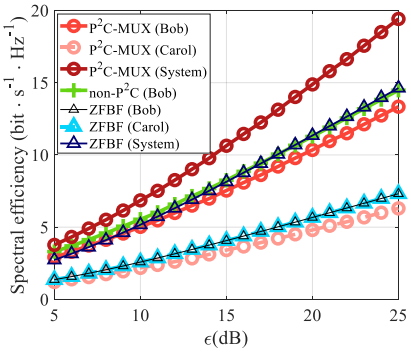

Fig. 7. Comparison of SE under various mechanisms.

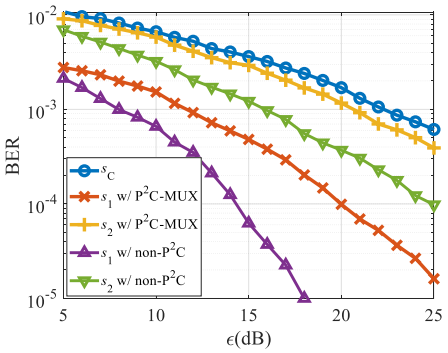

Fig. 8. BER of ECSs and ACS detection under various schemes.

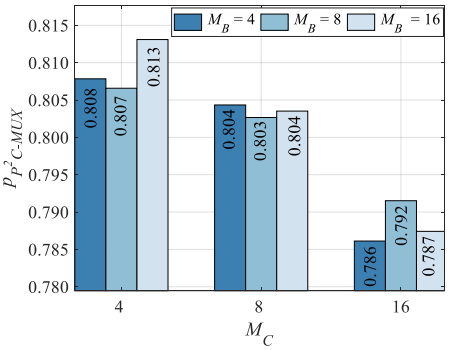

Fig. 9. Impact of M_B and M_C on p_{P^2C-MUX} under $N = 4$, $K = 2$, and $U = 1$.

of non-P^{2}C is solely determined by Bob's SE. In both ZFBF and the non-P^{2}C scheme, equal power is allocated to the two data streams sent from Alice.

Fig. 7 plots the variation of the SE of Carol, Bob, and the overall system with respect to ϵ under different transmission schemes. In the non-P^{2}C scheme, the system SE is equal to Bob's SE, as no ACS is transmitted to Carol. As the figure shows, non-P^{2}C achieves the highest SE for Bob, while P^{2}C-MUX demonstrates comparable performance, with ZFBF performing the worst. This performance disparity arises because, under ZFBF, Alice transmits only a single data stream to Bob. Furthermore, when designing the precoding vector for Bob, Alice must avoid causing interference to Carol, which can lead to a mismatch between the precoded signal and $\mathbf{H}_{AB}$, thus reducing Bob's SE. In contrast, both non-P^{2}C and P^{2}C-MUX allow the transmission of two parallel data streams from Alice to Bob in a point-to-point MIMO manner, enabling a higher SE for Bob. However, since P^{2}C-MUX utilizes PowC to generate the ACS, it incurs a slight loss in SE compared to non-P^{2}C.

As for Carol's SE, ZFBF yields the best performance, followed by P^{2}C-MUX. Since non-P^{2}C is unable to provide data service to Carol, her SE is 0, and we omit this curve for simplicity. Moreover, under P^{2}C-MUX Alice's precoding is based on $\mathbf{H}_{AB}$ rather than $\mathbf{H}_{AC}$, while Carol's reception performance depends on $\mathbf{H}_{AC}$, which is independent of $\mathbf{H}_{AB}$. This can further lower the desired signal quality at Carol. Consequently, the SE achieved at Carol under ZFBF surpasses that of P^{2}C-MUX.

As for system SE, P^{2}C-MUX demonstrates the best performance, followed by non-P^{2}C, while ZFBF exhibits the lowest. This is because P^{2}C-MUX leverages the two ECSs to produce a desired ACS at Carol, thereby supporting three concurrent data transmissions simultaneously. In contrast, both non-P^{2}C and ZFBF can only provide two simultaneous data transmissions, yielding a relatively lower system SE. Therefore, P^{2}C-MUX can significantly enhance system SE without incurring additional power or antenna overhead.

Next, we proceed to simulate the bit error rate (BER) of the two ECSs received by Bob and the ACS received by Carol under P^{2}C-MUX and non-P^{2}C, respectively, as illustrated in Fig. 8. When using P^{2}C-MUX, we label the BER curves of Bob's two ECSs as "s_1 w/ P^{2}C-MUX" and "s_2 w/ P^{2}C-MUX", respectively, while BER of Carol's ACS is labeled as "s_C". Similarly, under non-P^{2}C, BER curves of Bob's two ECSs are labeled with "s_1 w/ non-P^{2}C" and "s_2 w/ non-P^{2}C." Both Bob and Carol employ maximum likelihood (ML) detection to demodulate their respective data symbols, and the number of error bits is counted accordingly.

As Fig. 8 shows, compared to non-P^{2}C, P^{2}C-MUX results in an increased BER for both ECSs at Bob. This degradation arises from the power adjustment applied to the ECSs in P^{2}C-MUX. Unlike non-P^{2}C, which adopts equal power allocation, P^{2}C-MUX employs distinct power coefficients to modify the ECSs. So, the transmission associated with a smaller power coefficient experiences a higher BER due to reduced signal power. Although the transmission with a larger power coefficient can yield a lower BER, the overall BER is dominated by the transmission with the higher BER. As a result, P^{2}C-MUX achieves a moderate increase in the BER performance.

In what follows, we evaluate the feasible probability of the P^{2}C-MUX (denoted as p_{P^2C-MUX}) under various values of N, K, U, M_B, and M_C. For simplicity, we have all ECSs employ M_BPSK, while all ACSs adopt M_CPSK, respectively. We set $N \in \{3,4,5,6\}$, $M_B, M_C \in \{4,8,16\}$, $K \in \{1,2,3\}$, $U \in \{1,2,3\}$, and $\epsilon = 5$dB. Fig. 9 shows the impact of M_B and M_C on p_{P^2C-MUX} when $N = 4$, $K = 2$, and $U = 1$. As the figure shows, for a fixed M_C, varying M_B does not significantly affect p_{P^2C-MUX}. This phenomenon is attributed to the mismatch between $\mathbf{H}_{AC}$ and the characteristics of ECSs, causing the ECSs arriving at Carol to experience a stochastically lower channel gain than those at Bob. A detailed analysis can be found in Section IV-B. On the other hand, for a fixed M_B, an increase in M_C leads to a decrease in p_{P^2C-MUX}. This is because a larger M_C yields greater diversity among the constellation points of the ACS, which increases the likelihood that no solution exists for $\boldsymbol{\alpha}$ and $\boldsymbol{\kappa}$ that simultaneously satisfy the demands of $K = 2$ additional Rxs, thus reducing p_{P^2C-MUX}.

Fig. 10 illustrates the impact of N on p_{P^2C-MUX} under $M_B = M_C = 4$, $K = 2$, and $U = 1$. As the figure shows, p_{P^2C-MUX} increases as N grows. This is because, as the number of ECSs increases, their combinations become more

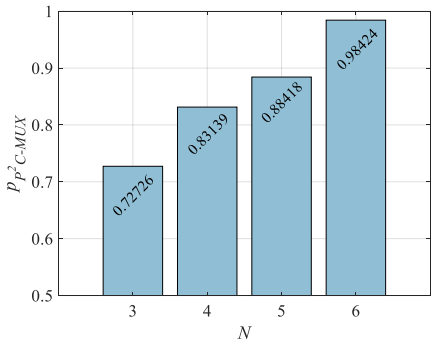

Fig. 10. Impact of N on p_{P^2C-MUX} under $M_B = M_C = 4$, $K = 2$, and $U = 1$.

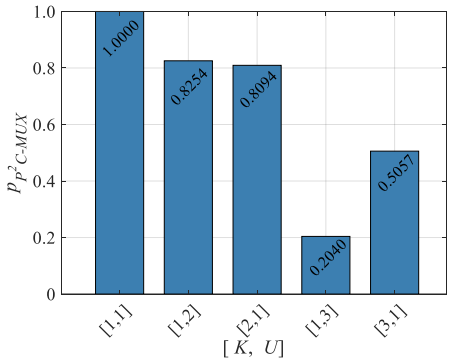

Fig. 11. Impact of K and U on p_{P^2C-MUX} under $M_B = M_C = 4$, and $N = 4$.

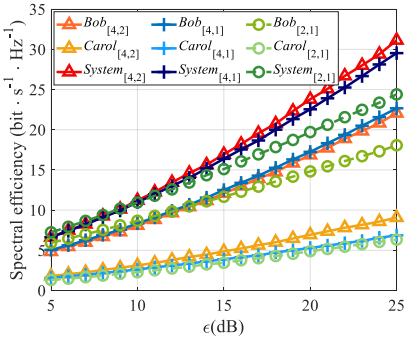

Fig. 12. SE of P^{2}C−MUX under different values of N and U.

diverse, thus enhancing the probability that the desired ACSs can be successfully generated by the ECSs.

Fig. 11 shows the impact of K and U on p_{P^2C-MUX} under $N = 4$ and $M_B = M_C = 4$. For clarity, we define the pair of K and U as a parameter set $[K, U]$ and adopt $[K, U] \in \{[1,1],[1,2],[2,1],[1,3],[3,1]\}$ in the simulation. As the figure shows, p_{P^2C-MUX} decreases as either K or U increases. This is because, for a fixed N, increasing the number of ACSs (i.e., larger K and U) raises the likelihood that P^{2}C−MUX has no feasible solution for $\boldsymbol{\alpha}$ and $\boldsymbol{\kappa}$. A detailed analysis can be found in Section IV-B.

Since the parameters N, K, and U affect p_{P^2C-MUX}, they consequently influence the average SE of P^{2}C−MUX. Therefore, we investigate the impact of these parameters on the SE of Bob, Carol, and the overall system, as plotted in Fig. 12. Since both K and U exert a similar influence on p_{P^2C-MUX}, which can be observed from Fig. 11, we fix $K = 1$ and vary U in the simulation of Fig. 12. Moreover, we set $N_A = N_B = 4$, $N_C = 2$, $K = 1$, $M_B = M_C = 4$, $N \in \{2, 4\}$, and $U \in \{1, 2\}$ in the simulation. For ease of presentation, we define the pair of N and U as the parameter set $[N, U]$. Accordingly, we can label the SE yielded by P^{2}C−MUX as $\mathcal{N}_{[N,U]}$ where $\mathcal{N} \in \{Bob, Carol, System\}$. In the simulation, when no feasible solution of $\boldsymbol{\alpha}$ and $\boldsymbol{\kappa}$ exists for P^{2}C−MUX Alice is unable to provide additional data services to Carol, and we record Carol's SE as 0. In this case, Alice equally distributes her transmit power among the ECSs, causing P^{2}C−MUX to degenerate into the non-P^{2}C scheme.

As Fig. 12 plots, $System_{[4,2]}$ achieves the highest system SE, followed by $System_{[4,1]}$, while $System_{[2,1]}$ exhibits the lowest. This is analyzed as follows. On one hand, Bob receives four ECSs when $[N, U] \in \{[4,2],[4,1]\}$, which is twice the number of ECSs he receives under $[N, U] = [2, 1]$. Consequently, both $Bob_{[4,2]}$ and $Bob_{[4,1]}$ have significantly higher SE than $Bob_{[2,1]}$. Furthermore, since N is fixed in the simulations of $Bob_{[4,2]}$ and $Bob_{[4,1]}$, they exhibit a similar SE performance. On the other hand, Carol's SE benefits from a larger value of U, and therefore, $Carol_{[4,2]}$ outperforms $Carol_{[4,1]}$. Moreover, when $U = 1$, $p_{P^2C-MUX} = 1$ holds, hence both $Carol_{[4,1]}$ and $Carol_{[2,1]}$ yield similar SE performance. Based on the above analysis of Bob's and Carol's SE performance under various $[N, U]$ configurations, we can conclude that $System_{[4,2]}$ outputs the highest SE, followed by $System_{[4,1]}$, while $System_{[2,1]}$ exhibits the lowest.

Note that the results in Fig. 12 do not imply that increasing N and U will necessarily lead to improved system SE with P^{2}C−MUX. This is because p_{P^2C-MUX} has a significant impact on both Carol's SE and P^{2}C−MUX's system SE. When p_{P^2C-MUX} is low, the likelihood that Alice fails to serve Carol increases, resulting in Carol's SE being 0 with high probability, and Bob's SE reverts to that of point-to-point MIMO. As shown in Fig. 12, when N is fixed, Bob's SE with P^{2}C−MUX is not much different from that of non-P^{2}C. In such cases, if Carol's SE frequently drops to 0, the system SE will inevitably decline.

In summary, according to Figs. 10 and 11, larger values of N/U or N/K can yield higher p_{P^2C-MUX}, thus enhancing P^{2}C−MUX's SE.

VI. Conclusion

In this paper, we have proposed a *Power and Polarity Coding Assisted Multiplexing* (P^{2}C−MUX) method to enhance transmission efficiency by utilizing existing communication signals to create additional data transmissions, without incurring extra power and antenna overheads. Our comprehensive analysis, experimentation, and in-depth simulation results have demonstrated the validity and effectiveness of P^{2}C−MUX in achieving a higher system spectral efficiency over SOTA mechanisms.

Acknowledgments

This work is supported in part by the National Natural Science Foundation of China under Grant 62072351, Grant U23A20300, Grant 62202359, in part by the 111 Center under Grant B16037, in part by JSPS KAKENHI under Grant JP25K15087, in part by the Science and Technology Research Project of Henan Province under Grant 252102211120, in part by the Project of Cyber Security Establishment with Inter-University Cooperation, in part by the Key Research Project of Shaanxi Natural Science Foundation under Grant 2023-JC-ZD-35, and in part by the U.S. National Science Foundation under Grant 2245223.

REFERENCES

[1] K. B. Letaief, W. Chen, Y. Shi, et al., "The Roadmap to 6G: AI empowered Wireless Networks," *IEEE Commun. Mag.*, vol. 57, no. 8, pp. 84-90, 2019.

[2] K. Zheng, L. Zhao, J. Mei, et al., "Survey of Large-Scale MIMO Systems," *IEEE Commun. Surveys & Tut.*, vol. 17, no. 3, pp. 1738-1760, 2015.

[3] E. G. Larsson, O. Edfors, F. Tufvesson, et al., "Massive MIMO for Next Generation Wireless Systems," *IEEE Commun. Mag.*, vol. 52, no. 2, pp. 186-195, 2014.

[4] E. Telatar, "Capacity of Multi-Antenna Gaussian Channels," *AT&T-Bell Labs Internal Tech. Memo.*, vol. 10, no. 6, pp. 585-595, 1999.

[5] G. J. Foschini and M. J. Gans, "On Limits of Wireless Communications in a Fading Environment When Using Multiple Antennas," *Wirelss Personal Commun.*, vol. 6, no. 3, pp. 311-335, 1998.

[6] M. Vaezi, R. Schober, Z. Ding, et al., "Non-Orthogonal Multiple Access: Common Myths and Critical Questions," *IEEE Wireless Commun.*, vol. 26, no. 5, pp. 174-180, 2019.

[7] S. M. R. Islam, N. Avazov, O. A. Dobre, et al., "Power-Domain Non-Orthogonal Multiple Access (NOMA) in 5G Systems: Potentials and Challenges," *IEEE Commun. Surveys & Tut*., vol. 19, no. 2, pp. 721-742, 2016.

[8] J. Choi, "NOMA: Principles and Recent Results," in *Proc. Int. Symp. Wireless Commum. Syst. (ISWCS)*, pp. 349-354, 2017.

[9] P. Wang, L. Liu, S. Zhou, et al., "Near-Optimal MIMO-SCMA Uplink Detection With Low-Complexity Expectation Propagation," *IEEE Trans. Wireless Commun.*, vol. 19, no. 2, pp. 1025-1037, 2019.

[10] A. Tusha and H. Arslan, "Interference Burden in Wireless Communications: A Comprehensive Survey from PHY Layer Perspective," *IEEE Commun. Surveys & Tut.*, Early Access, 2024.

[11] N. Lee and R. W. Heath Jr, "Advanced Interference Management Technique: Potentials and Limitations," *IEEE Wireless Commun.*, vol. 23, no. 3, pp. 30-38, 2016.

[12] Z. Li, J. Chen, K. G. Shin, et al., "Interference Recycling: Exploiting Interfering Signals to Enhance Data Transmission," in *Proc. IEEE Conf. Comput. Commun. (INFOCOM)*, pp. 100-108, 2019.

[13] Z. Li, S. Le, J. Chen, et al., "Decomposed and Distributed Modulation to Achieve Secure Transmission," *IEEE Trans. Mobile Comput.*, vol. 23, no. 12, pp. 11172-11190, 2024.

[14] D. Tse and P. Viswanath, "Fundamentals of wireless communication," Cambridge university press, 2005.

[15] V. Jungnickel, K. Manolakis, S. Jaeckel, et al., "Backhaul Requirements for Inter-site Cooperation in Heterogeneous LTE-Advanced Networks," in *Proc. IEEE Int. Conf. Commun. (ICC)*, pp. 905-910, 2013.

[16] I. F. Akyildiz, D. M. Gutierrez-Estevez, R. Balakrishnan, et al., "LTE-Advanced and the Evolution to Beyond 4G (B4G) Systems," *Physical Commun.*, vol. 10, pp. 31-60, 2014.

[17] Z. Li, C. Liu, L. Zhang, et al., "Exploiting Interference With an Intelligent Reflecting Surface to Enhance Data Transmission," *IEEE Trans. Wireless Commun.*, vol. 23, no. 8, pp. 9776-9792, 2024.

[18] Z. Li, Y. Liu, K. G. Shin, et al., "Design and Adaptation of Multi-Interference Steering," *IEEE Trans. Wireless Commun.*, vol. 18, no. 7, pp. 3329-3346, 2019.